GI_Forum 2021, Issue 1
Page: 39 - 45
Research Paper
Corresponding Author:
sepideh.tavakkoli-piralilou@stud.sbg.ac.at
DOI: 10.1553/giscience2021_01_s39

Automatic Landslide Detection Using Bi-Temporal Sentinel 2 Imagery

Sepideh Tavakkoli Piralilou[1], Hejar Shahabi[2,3] and Robert Pazur[2,4]

[1]University of Salzburg, Austria
[2]Slovak Academy of Sciences, Slovakia
[3]University of Tabriz, Iran
[4]Swiss Federal Institute for Forest, Snow and Landscape Research WSL, Switzerland

Abstract

Landslide inventory data sets are required for any landslide susceptibility mapping and prediction approaches. However, generating accurate landslide inventory data sets depends on applied methods and quality of input data, for example spatial resolution for satellite imagery. Therefore, the accuracy and availability of inventories vary in different studies. This study evaluated a strategy of sudden landslide identification product (SLIP) for landslide detection using Bi-Temporal Sentinel 2 Imagery and ALOS Digital Elevation Model (DEM). The resulting landslide detection map was then compared with an improved version of SLIP based on a fuzzy overlay. The resulting probability map was classified into three classes using the natural breaks method; the third class with the highest probability was extracted as the final map. The accuracy assessment stage demonstrated that using the improved version increased the accuracy by 16% compared to the SLIP method.

Keywords: earth observation, sudden landslide identification product (SLIP), Sentinel 2

1 Introduction

Landslides are the most dangerous and unpredictable natural hazards that usually result in severe destructions, damaging natural resources, and loss of human life and property (Hölbling et al., 2015). They occur in different types, frequencies, and intensities worldwide (Ngo et al, 2020 and Ghorbanzadeh et al., 2019A). Seeking suitable solutions to prevent and mitigate its calamitous consequences is, therefore, a high priority for society. Recent advances in remote sensing, increasing availability of Earth observation data, and progress in semi-automated and automated techniques enable the monitoring and analysis of large areas. In this regard, many machine learning (ML) methods and procedures have been developed and applied for landslide inventory mapping from different satellite imageries (Ghorbanzadeh et al., 2019B and Ghorbanzadeh et al., 2020). The ML methods are categorized into two main groups of supervised and unsupervised techniques (Mou et al., 2017). In supervised methods and model selection, the training dataset plays a vital role in mapping landslides, and the performance and accuracy of the model have a strong correlation with the quantity and quality of training data

(Ghorbanzadeh et al., 2020 and Hölbling 2012). In the unsupervised methods, pixels that share similar spectral characteristics are grouped as a cluster, and the similarity threshold is usually defined by the user (Tran et al., 2019). The standard unsupervised methods are K-means clustering or Interactive self-organization data analysis (ISODATA) (Karami et al., 2015 and Abburu et al., 2015). Although they are easy to apply and do not require any labelled data for classification and clustering data, their resulting classification accuracy is usually lower than supervised approaches.

For the case of bi-temporal images, some techniques, including image differencing, normalized difference vegetation index (NDVI), change vector analysis (CVA), spectral features variance, and image rationing has been applied for land surface change detection and landslide detection in particular (Vázquez-Jiménez et al., 2018, Ramos-Bernal et al., 2018 and Solano-Correa et al., 2018). In these techniques, mapping land surface changes or deformation caused by landslide phenomena is more achievable, but selecting the optimal thresholds to classify or separate change from no-change is still a challenge (Panuju et al., 2020).

In this study, we followed a sudden landslide identification product (SLIP) strategy to overcome the thresholding issue for landslide detection using bi-temporal images. SLIP combines multiple related spectral channels from bi-temporal images to estimate landscape changes. In this regard, we examined image indices such as red change (Fayne et al., 2019) and modified normalized multiband drought index (mNMDI) and fuzzy overlay to automatically detect and classify landslides without introducing any thresholds to data.

2 Study area

The chosen study area for this investigation is Eastern Iburi, which is in Hokkaido, Japan (see figure 1). On September 6th, 2018, an earthquake struck Eastern Iburi with a magnitude of 6.6 (Mw), resulting in the deaths of 41 people; 36 of the victims were perished by landslides (Yamagishi et al., 2018). Nearly 5600 landslides, primarily shallow, were caused by the earthquake equal to an area of 46.3 km^2. However, the main reason for such a copious number of landslides was that the day before the earthquake, typhoon Jebi brought torrential rainfalls into the region, making the area highly susceptible to landslides (Osanai et al., 219). A landslide inventory map in this region is generated by the Geographical Survey Institute (GSI) of Japan. It is used as a perfect reference map to evaluate the accuracy of our method in landslide detection. More details on the landslide inventory map are available in Zhang et al., 2019.

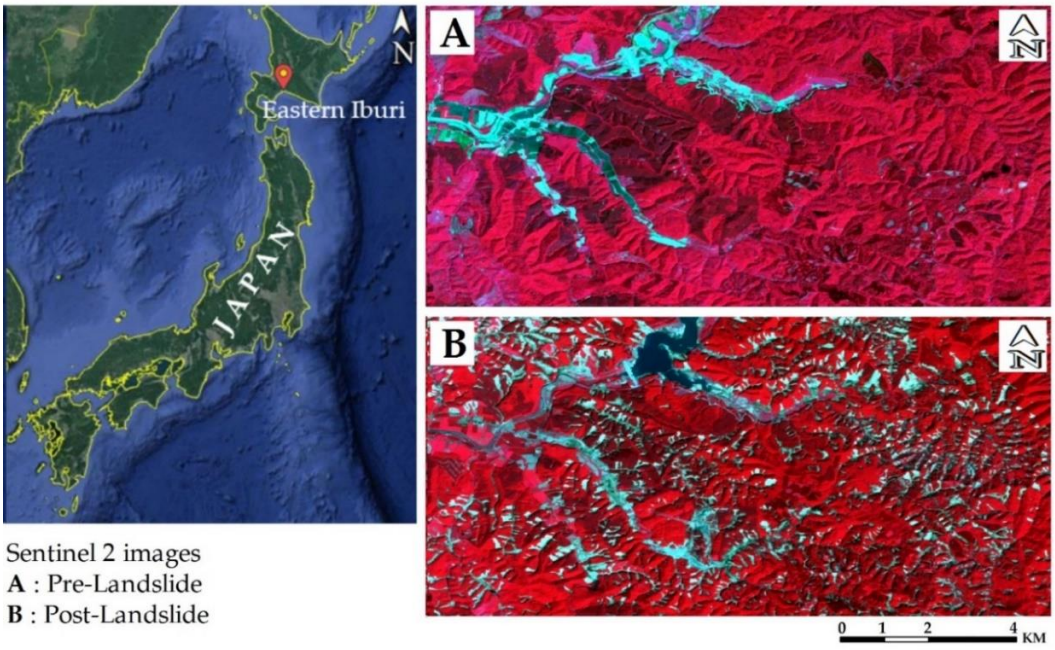

Figure 1: The location of our case study area of Eastern Iburi in Hokkaido, Japan. Pre and post landslide Sentinel-2 images are presented by the band combination 8-4-3 (NIR, Red, Green).

3 Data and methodology

In this study, Sentinel 2A images were acquired for dates before and after the landslide event. Based on the SLIP method, we used a stack of five images that had cloud cover less than 10% for both the pre-landslide image and post-landslide image. Before using these datasets for landslide mapping, Sen2Cor (Main-Knorn et al., 2017) plugin, which is available for SNAP software, was used to apply atmospheric corrections. Besides, since the slope is an essential factor in detecting landslides (Ghorbanzadeh et al., 2019B), we used 12-meter ALOS Digital Elevation Model to generate a slope layer used with satellite images. Sentinel 2A images include 13 bands with a spatial resolution ranging from 10 to 60 meters. Furthermore, all images and slope layers were resampled to 10-meter resolution in QGIS software for further analysis.

3.1 Sudden Landslide Identification Product (SLIP)

The research methodology established based on a change detection algorithm called SLIP proposed by Fayne, et al. (2019) utilizes Landsat-8 multispectral images and elevation data from the Shuttle Radar Topography Mission to detect landslides. In SLIP there are two crucial indices called Red Change and Normalized Multiband Drought Index (NMDI) that directly impact detecting landslides. The former index calculates the ratio of changes in Red bands (655 nm) in pre and post landslide images, expressed as equation 1, to map soil exposure. The

latter index is mainly used for measuring drought and flood conditions. It is sensitive to soil moisture and vegetation [15], making it an ideal tool to evaluate and map soil moisture changes. NMDI (Equation 2) is firstly created for MODIS multispectral data, but its performance was reported insufficient for landslide detection tasks; the authors modified (Equation 3 to be applicable) on Landsat-8 data for landslide detection. For Red change index, areas with more than a 40% increase in red reflectance were labelled as one and areas below the threshold were marked as zero. Also, mNMDI was calculated for pre and post landslide images and then using Spectral Characteristics Viewer from the U.S. Geological Survey mNMDI maps converted to binary maps with soil moisture one and without soil moisture zero. By subtracting post and pre-binary mNMDI maps, a change detection map with values -1, 0, and 1 is created, and then all values less than one are labelled as zero.

$$\text{Red Change} = \frac{(\text{R655}\ post - \text{R655}\ pre)}{\text{R655}\ pre} * 100 \quad (1)$$

$$\text{NMDI} = \frac{(\text{R}\ 860nm - (\text{R}\ 1640nm - \text{R}\ 2130nm)}{(\text{R}\ 860nm + (\text{R}\ 1640nm - \text{R}\ 2130nm)} \quad (2)$$

$$\text{mNMDI} = \frac{(\text{R}\ 860nm - \text{R}\ 2200nm)}{(\text{R}\ 860nm + \text{R}\ 2200nm)} \quad (3)$$

Moreover, the slope is another essential factor that authors used for mapping landslides. In SLIP, the slope is reclassified between zero and three based on the susceptibility to landslide; the higher susceptivity, the higher value, and vice versa. The remaining areas with values close to three show a high probability of being landslide, and values less than two indicate no landslide. The selection of thresholds and reclassification in the SLIP case study was based on the study site's topographical and physical characteristics.

3.2 Improved Sudden Landslide Identification Product (ISLIP)

In this section, we introduce ISLIP as an enhanced version of SLIP for landslide detection. In SLIP, the Landsat-8 multispectral data is used, while in ISLIP, we use Sentinel-2 images bands that have a similar wavelength as Landsat-8 bands for indices such as Red Change and mNMDI. However, in SLIP, the Red Change index can have infinite values, but in our method, we standardized it (Equation 4) between 0 and 1. Furthermore, we calculated mNMDI using the similar Sentinel 2 bands, and in our case, the values ranged between -1 and 1. The slope layer also was fuzzified between zero and one based on the vulnerability of landslide in our study area. To transform all layers into the same scale, we first subtracted pre-landslide mNMDI from post-landslide mNMDI, then fuzzified simply using linear fuzzy membership in QGIS, values close to 1 allocated higher membership and vice versa.

$$\text{Modified Red Change} = \frac{(\text{R665}\ post - \text{R665}\ pre)}{(\text{R665}\ post + \text{R665}\ pre)} \quad (4)$$

To detect landslides without introducing any thresholds, "AND" fuzzy overlay operators were used to combining all three layers, and then using the natural break clustering method, overlay map clustered into three classes.

4 Results

Represented in figure 2 are the resulting red change, pre and post landslide mNMDI indices, and mNMDI change map. According to the red change map (figure 2A), where landslides occurred, high positive values indicate changes from vegetation to bare soil due to landslide. For negative values, it shows the transformation from more minor moisturized areas to areas with high moisture like vegetation or water bodies. Moreover, in the pre-landslide mNMDI map (figure 2C), areas covered with dense vegetation show higher values, while low and negative values represent farms, bare lands, and dry soils. However, in the post-landslide mNMDI map (figure 2B), due to landslides and high soil exposure, the spatial distribution of values close to zero became frequent. Finally, in the change detection map (figure 2D), areas with more changes are associated with high positive values, and it is due to the subtraction of pre-landslide mNMDI from the post-landslide mNMDI map. Finally, the resulting map of applying the "AND" fuzzy operator on all three fuzzified inputs (Red Change, mNMDI change map, and slope) shows the probability of being a landslide ranges between zero and one; the higher values, the higher probability of being landslide. The output map is clustered into three classes, and the third class with the highest landslide probability was able to identify landslides with high accuracy. To compare our result with the SLIP method, we also mapped landslides using the SLIP method based on the procedure mentioned in [15], and pixels with values higher than 2.4 were selected as landslides.

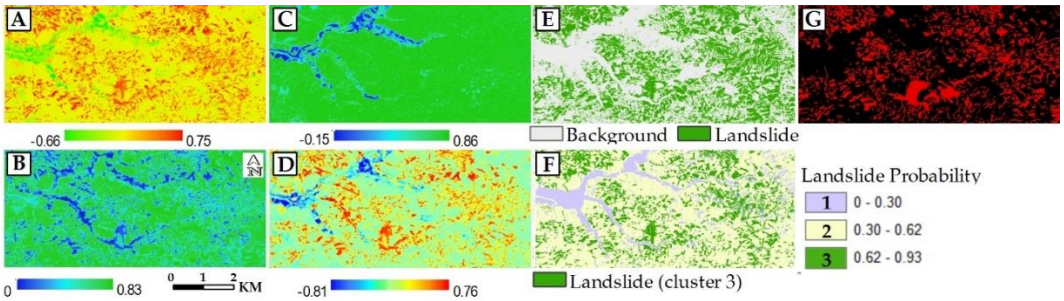

Figure 2: Spectral indices generated from Sentinel 2 images. Maps stand for (A) Red Change, (B) pre-landslide mNMDI, (C) post-landslide mNMDI, (D) mNMDI change map, (E) detected landslides (using SLIP), (F) detected landslides (using ISLIP), and (G) inventory map. Also, Maps from A to D are non-fuzzified layers and presented to indicate the indices change before and after landslide events.

5 Accuracy assessment and discussion

The resulting maps of areas detected as landslides were compared with the ground truth landslide inventory to calculate the precision accuracy assessment metric. The precision metric indicates the proportion of regions, which are correctly detected as landslide areas. Quantitative accuracy assessment using the landslide inventory map (figure 2, G) showed that ISLIP method could see landslides with an accuracy of 72%, while the SLIP method was 58% accurate. Therefore, the ISLIP has a better performance in landslide detection. One of the

factors that helped us achieve higher accuracy compared to the SLIP method is the higher spatial resolution of Sentinel-2A images.

The ISLIP algorithm shows how freely available Sentinel 2A images can be used for automated and landslide detection. However, the applied algorithms' transferability on the other regions is still considered a limitation of this study. The algorithms map changes on the surface within areas with high slopes. Thus, the slope factor played an important role in identifying the landslides, and the wrong fuzzification of the slope factor can result in a systematic bias in detecting landslides. Also, these algorithms may not be demonstrating the same accuracy for the landslides that covered by vegetation after the event.

6 Conclusions

The applied SLIP and ISLIP could automatically detect landslides to reduce the amount of time needed to analyze satellite imagery manually. This algorithm examined a large area and could show an acceptable accuracy compared to the current supervised classification models, which can be considered a practical approach in landslide research.

References

Hölbling, D., et al. *Object-based landslide mapping on satellite images from different sensors*. in *EGU General Assembly Conference Abstracts*. 2015.

Ngo, P.T.T., et al., *Evaluation of deep learning algorithms for national scale landslide susceptibility mapping of Iran.* Geoscience Frontiers, 2020. **12**(2): p. 505-519.

Ghorbanzadeh, O. and T. Blaschke. *Optimizing Sample Patches Selection of CNN to Improve the mIOU on Landslide Detection*. in *GISTAM*. 2019.

Ghorbanzadeh, O., et al., *Evaluation of Different Machine Learning Methods and Deep-Learning Convolutional Neural Networks for Landslide Detection.* Remote Sensing, 2019. **11**(2): p. 196.

Ghorbanzadeh, O., et al., *Landslide Mapping Using Two Main Deep-Learning Convolution Neural Network (CNN) Streams Combined by the Dempster—Shafer (DS) model.* IEEE Journal of Selected Topics in Applied Earth Observations and Remote Sensing, 2020.

Mou, L., P. Ghamisi, and X.X. Zhu, *Unsupervised spectral–spatial feature learning via deep residual Conv–Deconv network for hyperspectral image classification.* IEEE Transactions on Geoscience and Remote Sensing, 2017. **56**(1): p. 391-406.

Hölbling, D., et al., *A semi-automated object-based approach for landslide detection validated by persistent scatterer interferometry measures and landslide inventories.* Remote Sensing, 2012. **4**(5): p. 1310-1336.

Tran, C.J., et al., *Unsupervised Classification for Landslide Detection from Airborne Laser Scanning.* Geosciences, 2019. **9**(5): p. 221.

Karami, A., et al., *Gully erosion mapping using object-based and pixel-based image classification methods.* Environmental & Engineering Geoscience, 2015. **21**(2): p. 101-110.

Abburu, S. and S.B. Golla, *Satellite image classification methods and techniques: A review.* International journal of computer applications, 2015. **119**(8).

Vázquez-Jiménez, R., et al., *Thresholding algorithm optimization for change detection to satellite imagery*, in *Colorimetry Image Processing*. 2018, InTech.

Ramos-Bernal, R.N., et al., *Evaluation of unsupervised change detection methods applied to landslide inventory mapping using ASTER imagery.* Remote Sensing, 2018. **10**(12): p. 1987.

Solano-Correa, Y.T., F. Bovolo, and L. Bruzzone, *An approach for unsupervised change detection in multitemporal VHR images acquired by different multispectral sensors.* Remote Sensing, 2018. **10**(4): p. 533.

Panuju, D.R., D.J. Paull, and A.L. Griffin, *Change Detection Techniques Based on Multispectral Images for Investigating Land Cover Dynamics.* Remote Sensing, 2020. **12**(11): p. 1781.

Fayne, J.V., et al., *Automated Satellite-Based Landslide Identification Product for Nepal.* Earth Interactions, 2019. **23**(3): p. 1-21.

Yamagishi, H. and F. Yamazaki, *Landslides by the 2018 Hokkaido Iburi-Tobu Earthquake on September 6*. Landslides, 2018. **15**(12): p. 2521-2524.

Osanai, N., et al., *Characteristics of landslides caused by the 2018 Hokkaido Eastern Iburi Earthquake.* Landslides, 2019. **16**(8): p. 1517-1528.

Zhang, S., et al., *Characteristics of landslides triggered by the 2018 Hokkaido Eastern Iburi earthquake, Northern Japan.* Landslides, 2019. **16**(9): p. 1691-1708.

Main-Knorn, M., et al. *Sen2Cor for sentinel-2*. in *Image and Signal Processing for Remote Sensing XXIII*. 2017. International Society for Optics and Photonics.